Annals of Biomedical Engineering, Vol. 37, No. 9, September 2009 (© 2009) pp. 1781–1795
DOI: 10.1007/s10439-009-9743-9

Measurement of Solute Transport in the Endothelial Glycocalyx Using Indicator Dilution Techniques

LUJIA GAO and HERBERT H. LIPOWSKY

Department of Bioengineering, The Pennsylvania State University, 205 Hallowell Building, University Park, PA 16802, USA

(Received 23 January 2009; accepted 10 June 2009; published online 24 June 2009)

Abstract—A new method is presented to quantify changes in permeability of the endothelial glycocalyx to small solutes and fluid flow using techniques of indicator dilution. Following infusion of a bolus of fluorescent solutes (either FITC or FITC conjugated Dextran70) into the rat mesenteric circulation, its transient dispersion through post-capillary venules was recorded and analyzed offline. To represent dispersion of solute as a function of radial position in a microvessel, a virtual transit time (VTT) was calculated from the first moment of fluorescence intensity–time curves. Computer simulations and subsequent *in vivo* measurements showed that the radial gradient of VTT within the glycocalyx layer ($\Delta VTT/\Delta r$) may be related to the hydraulic resistance within the layer along the axial direction in a post-capillary venule and the effective diffusion coefficient within the glycocalyx. Modeling the inflammatory process by superfusion of the mesentery with 10^{-7} M fMLP, $\Delta VTT/\Delta r$ was found to decrease significantly from 0.23 ± 0.08 SD s/μm to 0.18 ± 0.09 SD s/μm. Computer simulations demonstrated that $\Delta VTT/\Delta r$ is principally determined by three independent variables: glycocalyx thickness (δ), hydraulic resistivity (K_r) and effective diffusion coefficient of the solute (D_{eff}) within the glycocalyx. Based upon these simulations, the measured 20% decrease in $\Delta VTT/\Delta r$ at the endothelial cell surface corresponds to a 20% increase in D_{eff} over a broad range in K_r, assuming a constant thickness δ. The absolute magnitude of D_{eff} required to match $\Delta VTT/\Delta r$ between *in vivo* measurements and simulations was found to be on the order of $2.5 \times 10^{-3} \times D_{free}$, where D_{free} is the diffusion coefficient of FITC in aqueous media. Thus the present method may provide a useful tool for elucidating structural and molecular alterations in the glycocalyx as occur with ischemia, metabolic and inflammatory events.

Keywords—Glycocalyx, Indicator dispersion, Solute transport, Diffusion coefficient, Hydraulic resistance.

Address correspondence to Herbert H. Lipowsky, Department of Bioengineering, The Pennsylvania State University, 205 Hallowell Building, University Park, PA 16802, USA. Electronic mail: hhlbio@engr.psu.edu, hhl2@psu.edu

INTRODUCTION

The endothelial glycocalyx is a negatively charged layer of proteins and polysaccharides coating the luminal surface of the vascular endothelium. First observed by Luft[11] in 1966 using electron microscopy following ruthenium red staining, the structure and function of the glycocalyx has become a subject of intense interest because of it role as barrier to transvascular exchange of macromolecules,[5] barrier to leukocyte-endothelial adhesion[15] and a depository for growth factors and enzymes.[26] These factors include anticoagulants antithrombin III, heparin cofactor II, thrombomodulin and tissue factor pathway inhibitor,[25] extracellular superoxide dismutase,[1] and possibly basic fibroblast growth factor (bFGF) and bFGF receptor.[38] Structurally, the glycocalyx is a three-dimensional mesh-like layer with a regular 20 μm repeating pattern in both axial and radial directions.[31] The repeating pattern arises from proteins decorated with chains of disaccharides that form the glycosaminoglycans (GAGs) heparan sulfate (HS), chondroitin sulfate (CS), keratan sulfate (KS), dermatan sulfate (DS) and hyaluronan (HA).[35] Among these polysaccharides, HS, CS and HA are the most abundant GAGs in the endothelial glycocalyx.[19] The GAGs HS and CS are attached to either transmembrane proteins (primarily the family of syndecans) or membrane bound lipid linked proteins (glypicans) whereas HA appears to form a loose meshwork held in place by a few linking proteins.[24] The mutually repulsive force of the negatively charged sulfated GAGs HS and CS appears to keep the glycocalyx from collapsing and attracts water molecules so that the glycocalyx can remain hydrated.

It has been found that components of the glycocalyx are shed under various pathological conditions, such as inflammation,[16] ischemia-reperfusion injury,[16] hyperglycemia,[40] and in the presence of oxidized low density lipoproteins.[4,34] Such shedding may play a significant role in progression of the inflammatory process by

exposing underlying cell adhesion molecules buried within the glycocalyx[26] or facilitate unabated progression of the coagulation process.[7]

Several studies have suggested that the presence of the glycocalyx may be hydrodynamically significant and play a profound role in affecting microvascular hemodynamics. *In situ* perfusion of the microvasculature with enzymes to strip off selected components of the glycocalyx have shown that capillary hematocrit may rise dramatically.[6] It has been suggested that a fall of intravascular resistance occurs due to cleavage of various glycans.[30] These hemodynamic effects may arise from an increase in the effective diameter of the microvessel lumen attendant to degradation of the glycocalyx or a decrease in retardation of plasma movement through the glycocalyx.

Measurements of the structural thickness of the glycocalyx have been fraught with difficulties and have revealed a large disparity between in vivo measurements in living tissue and high resolution microscopy of fixed tissues. Electron microscopy has revealed a thickness on the order of 100 nm.[3,11] In contrast, *in vivo* observations of the exclusion of red cells have revealed a thickness on the order of 500 nm.[35] Using techniques of micro-particle image velocimetry (PIV) extrapolation of near-wall velocity profiles to the EC surface of post-capillary venules has revealed the presence of a 300–400 nm thick surface layer.[29] Techniques of micro-PIV have also demonstrated the absence of a hydrodynamically significant layer on cultured EC's compared with *in vivo* cells (30 vs. 500 nm, respectively), thus emphasizing the need to acquire structural characteristics of the glycocalyx *in situ* in the living animal.[23]

The role of the glycocalyx as a barrier to transvascular fluid exchange has received considerable attention. Enzymatic degradation of the glycocalyx with pronase treatment has been shown to increase hydraulic conductivity (L_p) of the capillary[2] and the permeability to the macromolecules albumin and α-lactalbumin.[8] With the goal of integrating these observations into a structurally realistic model, the glycocalyx has been modeled as a Brinkman layer that resists the permeability to macromolecules as in a Darcy diffusion model, and with a resistance to fluid flow within the layer proportional to fluid velocity.[37]

Within this framework, the present study was undertaken to develop a method for characterizing the relative sensitivity to changes in thickness, solute diffusion coefficient and resistance to fluid movement during induced structural alterations *in vivo* in post-capillary venules. To this end, the transit of small solutes and macromolecules parallel to the EC wall of venules was quantified using techniques of indicator dispersion through the glycocalyx. Solute transport was evaluated under steady state (control) conditions and following stimulation of shedding of glycans from the endothelium with the chemoattractant f-met-leu-phe.[15] *In vivo* measurements of solute dispersion were related to structural and hydrodynamic characteristics of the glycocalyx with a finite element computational model.

EXPERIMENTAL METHODS

Technique of Indicator Dispersion

The flux of small solutes through the endothelial glycocalyx parallel to the wall of post-capillary venules was examined by infusion of a fluorescent indicator molecule (either low molecular weight fluoresceinisothiocyanate, FITC, or a high molecular weight fluoresceinated dextran 70 kDa, Dx70 Sigma, St. Louis, MO), into the microvasculature of intestinal mesentery of the rat. A small bolus, 0.02 mL, was injected proximal to the observation site by means of an indwelling catheter (PE10) in the ileocolic artery, as illustrated in Fig. 1a. Dispersion of the indicator was quantified by measurement of the intensity vs. time curves, $I(r, t)$, as a function of radial position (r) of the fluorescence emission as the bolus passed through a post-capillary venule. The dispersion was characterized

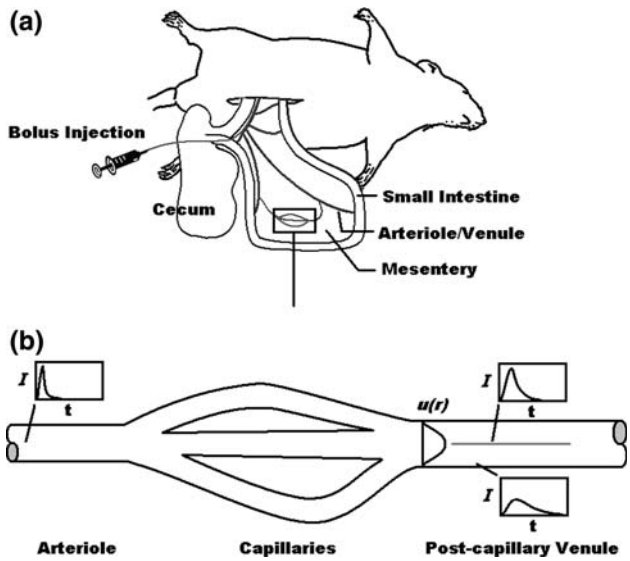

FIGURE 1. Schematic of experimental procedures: (a) A 20 μL bolus of fluorescent solutes (FITC or FITC-Dextran70) was injected into the ileocolic artery and its dispersion in the microvasculature was observed by intravital microscopy of the intestinal mesentery. (b) Intensity–time curves of the bolus were recorded in post-capillary venules, and digitized at each time step along a radial line while focused on the diametral plane, as illustrated for indicator-dispersion curves along the centerline and near the vessel wall.

by the first moment of the intensity–time curve, as typified by the classical Stewart–Hamilton method. For an indicator of infinitesimal volume and observed at a location where all of the indicator passes through the observation site, it has been shown that the first moment equals the mean transit time of indicator from injection to observation sites.[13] It has also been demonstrated that between multiple observation sites within the microvascular network, when conservation of mass between the sites is maintained the first moment may also provide a useful measure of the mean transit time between sites.[12] In the present approach, measurement of the first moment of the indicator at a specific radial position within a microvessel was interpreted as a virtual transit time, VTT(r), from an indeterminate source, as schematized in Fig. 1b, with its value obtained from:

$$\mathrm{VTT}(r) = \frac{\int_0^\infty I(r,t)\cdot t\cdot dt}{\int_0^\infty I(r,t)\cdot dt}. \quad (1)$$

As shown in the following experimental and computational models, the radial distribution of VTT(r) may be related to the diffusional characteristics of the indicator and the resistance to flow of its solvent as the indicator is transported through the endothelial glycocalyx.

Animal Preparation

Male Wistar rats, 200–300 g in weight, were anesthetized with sodium pentobarbital (45 mg/kg, i.p.). A tracheotomy was performed to permit spontaneous respiration. Supplemental doses of anesthetic (16.5 mg/mL) were administrated via an indwelling catheter in the right internal jugular vein to maintain a surgical plane of anesthesia. Arterial blood pressure was monitored through a second cannula in the right carotid artery that was connected to a strain-gage type pressure transducer. Body core temperature was maintained by a heating pad controlled by a close-loop automatic controller (FHC, Bowdoinham, ME). A mid-line incision was performed to exteriorize the terminal ileum which was draped over a clear glass pedestal for viewing by intravital microscopy. All exteriorized tissues were covered by sterile cotton gauze and superfused with Ringer's solution warmed to 37 °C. To deliver the fluorescent dye bolus, the ileocolic artery was separated from connective tissue and cannulated with PE-10 polyethylene tubing, which was connected to 250-μL delivery syringe (Hamilton). Bolus injections of either 0.1% FITC or 0.2% FITC-Dx70 (Sigma) in Ringer's solution, were freshly prepared and maintained at 37 °C by incubation in a hot water bath.

Experimental Instrumentation and Protocols

A well vascularized mesenteric window was viewed under either bright-field microscopy with trans-illumination (tungsten lamp) or fluorescence with incident fluorescence illumination using an Olympus-epifluorescence illuminator (Hg lamp) and dichroic mirrors suitable for visualization of the fluorescein emission spectrum. To induce changes in the composition of the glycocalyx, the tissue was superfused with 10^{-7} M *N*-formylmethionyl-leucyl-phenylalanine (fMLP, Sigma, St. Louis, MO) solubilized in Ringer's solution. This procedure has been shown to induce shedding of glycans from the surface of the endothelium via activation of G protein coupled receptors (GPCRs).[16]

Intra-Vital Microscopy

Post-capillary venules with diameters ranging from 25 to 45 μm were selected for observation with a water-immersion Zeiss 40x/0.75NA objective. The diameter of each venule was measured by the video image shearing technique (image shearing monitor, Model 908; IPM, San Diego, CA). The length of each venule in the field of view was approximately 85 μm. Red cell velocity (V_{RBC}) was measured along the centerline of each venule using the two-slit photometric technique with a self-tracking correlator (Model 204; IPM, San Diego, CA). The mean blood flow velocity was estimated from the equation $V_{\mathrm{MEAN}} = V_{\mathrm{RBC}}/1.6$.[10] The location for recording each bolus was chosen at least 15 vessel diameters away from the upstream bifurcation to allow complete mixing of the convergent streams. The propagation of each bolus was recorded using a low-light silicon-intensified target (SIT) camera (model 66; Dage-MTI, Michigan City, IN). For each recorded fluorescent bolus, a corresponding bright-field image was recorded to provide information on endothelial cell location. The transient progression of each bolus was recorded on SVHS video tape and digitized off-line at 640 × 480 pixels with a depth of 8 bits at 30 frames/s using a Scion LG-3 frame grabber (Scion, Frederick, MD). The digitized stack of TIFF images was de-interlaced by separating odd and even fields of each frame using a linear interpolation routine to provide a 60 field/s sampling interval. The digitized stack of images of each bolus had a spatial resolution of 7.53 pixels/μm.

Data Processing

For each venule, radial selection lines were drawn across the entire vessel lumen, normal to the direction of blood flow. Axial locations of selection lines were picked with the criterion that no adhered WBCs were

on the selection line. Intensity–time data sequences were recorded on each pixel of a selection line using the image processing software ImageJ (NIH, Bethesda, MD). All digitized intensities were corrected by subtraction of the background fluorescence obtained in the absence of fluorophore. Background fluorescence was digitized and averaged during the 10 to 15 video frames prior to the arrival of each bolus. Background fluorescence arose from the tissue autofluorescence and the presence of recirculating fluorescent molecules from prior infusions. After background correction, the virtual transit time was calculated for each pixel of the selection line using Eq. (1).

To establish a radial window of consistent size near the plasma membrane of the endothelium, within which the glycocalyx could potentially retard progression of the indicator, optical power (OP) was calculated from the intensity time curve at each radial position using the definition:

$$\mathrm{OP}(r) = \int_0^T (I(r,t) - I_{\mathrm{mean}}(r))^2 dt \tag{2}$$

where $I_{\mathrm{mean}}(r) = \frac{1}{T}\int_0^T I(r,t)\cdot dt$ is the time averaged fluorescence intensity and T is the duration of the bolus. The optical power varies with radius due to the transient quenching of the fluorescence as red blood cells pass a given axial station, and due to the transient intensity changes with varying concentration of the fluorophore. As shown in "Results," as the surface of the EC is approached along a radial line, OP(r) diminishes and an inflection point in OP(r) occurs as fluctuations in dye intensity from red cell passage begins to decrease relative to fluctuations arising from changes in dye concentration during passage of the bolus.

COMPUTATIONAL SIMULATION

To interpret the measurements of VTT(r) in terms of the permeability to solutes and the resistance to fluid transport within the glycocalyx, an annular core model of blood flow in a small bore tube of circular cross-section with three annuli was adopted. This model consisted of a central core of red cells ($0 \le r < r_c$) surrounded by an annulus of cell free plasma ($r_c \le r < r_g$) which was in turn surrounded by a porous layer lining the wall of the tube ($r_g \le r \le R$) which was representative of the glycocalyx of uniform thickness δ, where r_c, r_g and R are radial boundaries of the central core, glycocalyx and vessel wall, respectively.

Within the central red cell core and adjacent annular plasma layer, a two-layer model was adopted, following the model of Sharan and Popel.[28] The outer cell-free plasma layer spans from r_c to r_g, with apparent viscosity μ_p. Within the central core an apparent viscosity μ_c that was greater than μ_p was assumed, to account for the presence of red cells. Fluid flow within the glycocalyx was modeled as a two-dimensional flow field parallel to the wall as governed by the Brinkman equation.[27,37] The momentum conservation equations for these three layers are:

$$\begin{cases} \dfrac{\mu_c}{r}\dfrac{\partial}{\partial r}\left(r\dfrac{\partial u}{\partial r}\right) = \dfrac{\partial P}{\partial x} & 0 \le r < r_c \\ \dfrac{\mu_p}{r}\dfrac{\partial}{\partial r}\left(r\dfrac{\partial u}{\partial r}\right) = \dfrac{\partial P}{\partial x} & r_c \le r < r_g \\ \dfrac{\mu_p}{r}\dfrac{\partial}{\partial r}\left(r\dfrac{\partial u}{\partial r}\right) = \dfrac{\partial P}{\partial x} + K_r \cdot u & r_g \le r \le R \end{cases} \tag{3}$$

where r and x denote the coordinate system in radial and axial directions, respectively, u is the velocity in the axial direction, $\frac{\partial P}{\partial x}$ is the longitudinal pressure gradient, and K_r is the hydraulic resistivity within the glycocalyx. To implement the computations, a range of K_r from 10^4 to 10^{14} dyn·s/cm^4 was explored. A red cell core layer viscosity of $\mu_c = 3.84$ cP was computed using Eq. (4) (from Sharan and Popel[28]), assuming $Hc = 0.45$ within a post-capillary venule.[28]

$$\frac{\mu_c}{\mu_p} = 1 + 2.2\frac{(1-Hc)^{-0.8}-1}{(1-0.45)^{-0.8}-1} \tag{4}$$

The viscosity of plasma was taken as $\mu_p = 1.20$ cP.[20]

Solution of the system of Eq. (3) was implemented for the following boundary conditions:

(i) Axisymmetric flow along the vessel centerline,

$$\frac{\partial u}{\partial r} = 0, \quad \text{at } r = 0$$

(ii) No slip boundary at the blood vessel wall

$$u = 0, \quad \text{at } r = R, \text{ and}$$

(iii) No slip at adjacent layers

$$u_{r=r_{c-}} = u_{r=r_{c+}}$$
$$u_{r=r_{g-}} = u_{r=r_{g+}}$$

Mass Transport Model

The transient mass transfer of the dye bolus is affected by two processes: convection in the axial direction and diffusion in both radial and axial directions, as specified in the following equation,

$$\frac{\partial c}{\partial t} + u\frac{\partial c}{\partial x} = D_x\frac{\partial^2 c}{\partial x^2} + \frac{D_r}{r}\frac{\partial}{\partial r}\left(r\frac{\partial c}{\partial r}\right) \tag{5}$$

where c is the concentration of the indicator molecule as a function of time (t), radius (r) and length (x). D_x and D_r are the effective diffusion coefficients of the

indicator molecule in plasma in axial and radial directions, respectively. In the present study, the effective diffusion coefficient was assumed to be isotropic, $D_x = D_r = D$. However, the isotropic diffusion coefficient assumes different values for core, plasma layer and the glycocalyx layer. Diffusion coefficients in the core and plasma layer were taken as the free diffusion coefficient (D_{free}) of FITC in aqueous media 2.7×10^{-6} cm^2/s.[21] Although mixing effects of RBCs may contribute to a higher effective diffusion coefficient in the core layer, parametric numerical simulations indicated that the variation of diffusion coefficient in the core had minimal impact on the radial distribution of VTT. Similarly, varying the diffusion coefficient in the plasma layer by assuming a 90% reduction due to the presence of macromolecules, revealed less than a 5% reduction in the variation of VTT(r) with radial position near the EC.

Solution of the mass transfer equation was obtained with the boundary conditions:

(i) Axisymmetric flow along the vessel centerline

$$\frac{\partial c}{\partial r} = 0, \quad \text{at } r = 0$$

(ii) No flow transport normal to the vessel wall,

$$\frac{\partial c}{\partial r} = 0, \quad \text{at } r = R, \text{ and}$$

(iii) Well mixed entrance flow, with uniform concentration along the vessel radius which varied only as a prescribed function of time

$$c = c_{ent}, \quad \text{at } x = 0$$

where c_{ent} was taken from experimental recorded intensity time curves in the post-capillary venule.

Numerical Solution

The governing differential equations (Eqs. 3 and 5) were solved in a two-step process using the finite element solver of Comsol Multiphysics, version 3.5 (Comsol Inc., Burlington, MA) using a triangular mesh. The stationary velocity profile was computed by the built-in direct UMFPACK (Unsymmetric Multifrontal sparse LU Factorization Package) solver. The stationary velocity profile was stored and used to solve for transient concentration profiles using the UMFPACK linear solver.

The simulated length of a post-capillary venule was taken as 1 mm (>30 times diameter) to allow sufficient mixing. Vessel diameter was assumed to be 30 μm. Values for the cell-free plasma layer were obtained from *in vivo* measurements.

RESULTS

Measurements in Post-capillary Venules

Presented in Fig. 2 are brightfield and fluorescence images of a 30 μm diameter post-capillary venule as a bolus of FITC passes through the vessel. Fluorescence intensity along a radial measurement line was digitized to compute VTT(r) (Eq. 1) and optical power, OP(r) (Eq. 2). The boundaries of the red cell core, the endothelial cell (EC) surface, and the location of inflection points in OP(r) near the EC surface are shown. The surface of the EC was taken as the outermost edge of the dark refractive band that parallels the EC which is consistent with the surface upon which leukocytes can be clearly observed to roll. Average values of the thickness of the plasma layer between the edge of the RBC core and the EC surface are given in Table 1 for control and treatment conditions. No significant difference was found for location of the IP or

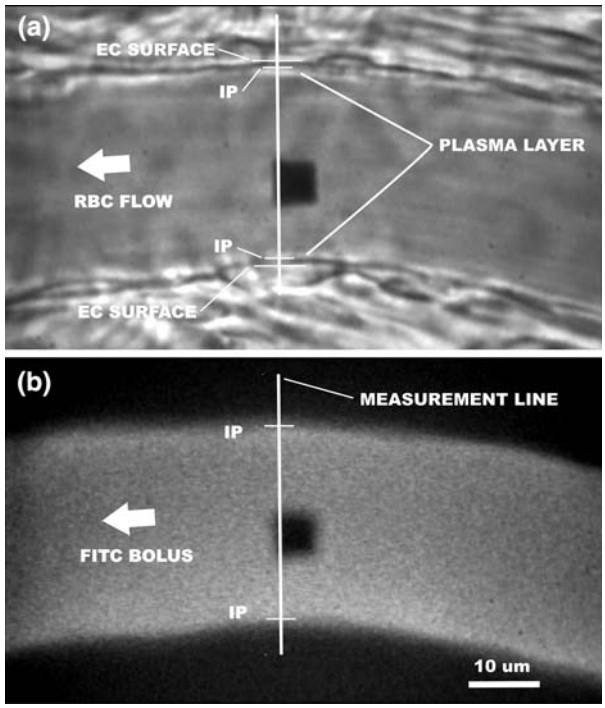

FIGURE 2. Intensity–time curves were measured along a line normal to the vessel longitudinal axis, shown above for (a) brightfield and (b) fluorescence images of a 30 μm diameter venule. The radial location of inflection points (IP) in the optical power and the endothelial cell (EC) surface are indicated by the short bars normal to the measurement line. The EC surface was taken at the outermost edge of the dark refractive band along the EC, which is consistent with the location of adhering and rolling leukocytes. The location of the IP is within the plasma layer, between the red blood cell column (*RBC*) and EC surface. The square black box in the center is the photodetector used for measurement of RBC velocity by the two-slit photometric method.

plasma layer thickness between control and fMLP for either FITC or Dx70.

Illustrated in Fig. 3 are representative intensity–time curves, $I(r, t)$, corresponding to each pixel along a radial measurement line, for dispersion of the bolus of FITC as shown in Fig. 2. At each radial position, the intensity–time curve appears as a log-normal shaped distribution. Near the wall of the venule ($r = R$) the glycocalyx layer appears to hinder progression of the bolus, as manifest by a delayed peak time and a prolonged and elevated tail. In the vicinity of the venule centerline ($r/R = 0$) light scattering by red cells results in a diminished peak intensity of the fluorescence emission at a given radius, which gives the bolus a parabolic appearance in the radial direction. Average red cell velocity within this venule equaled 3.0 mm/s. The transient intensities near the centerline of the venule were averaged radially over 5 adjacent pixels (~0.7 μm) to reduce noise and used as an input function for the computational model.

To explore the emission intensity distributions near the vessel wall in greater detail, shown in Fig. 4a is the radial distribution of $I(r, t)$ at the time at which intensity reaches a maximum and also for the time at which intensity at the wall reaches a maximum value for the 30 μm venule of Fig. 3. The vertical dashed lines in each panel represents the locations of the inflection points (IP) in the optical power (Eq. 4). Near the wall, both radial distributions exhibit similar slopes as the intensity diminishes with increasing distance from the luminal plasma layer. As shown in Fig. 4b, the total integrated mass flux $\left(\int_0^\infty I(r,t)dt\right)$ reveals a characteristic decrease in magnitude with radius in the vicinity of the wall which is indicative of dilution of the

TABLE 1. Measurements of the plasma layer thickness and inflection point location.

	FITC		Dextran-70	
Distance (μm)	Control	fMLP	Control	fMLP
n	51	51	27	27
Inflection point—EC surface	0.90 ± 0.25	0.93 ± 0.23	1.11 ± 0.25	1.10 ± 0.35
Red cell column—EC surface	1.77 ± 0.35	1.85 ± 0.58	1.97 ± 0.25	1.80 ± 0.38

Plasma layer thickness is defined as the distance between the edge of the RBC core and EC surface. Values shown are mean ± SD for *n* measurements in each treatment. Differences between control and fMLP were not statistically significant (*t*-test, $p > 0.5$).

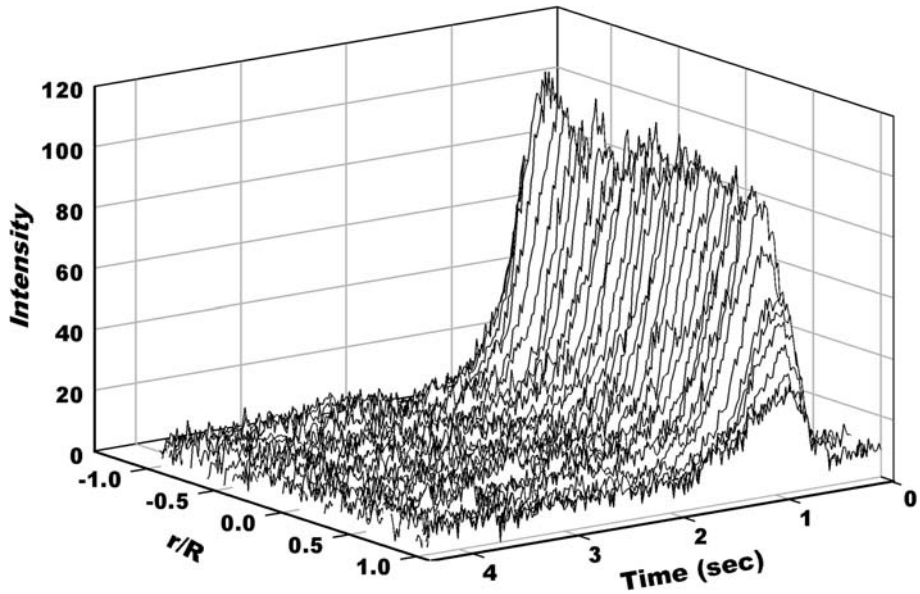

FIGURE 3. Representative intensity–time curves against radius for dispersion of a bolus of FITC in a 30 μm diameter venule with centerline red cell velocity of 1.5 mm/s. Fluorescence intensity was digitized using an 8-bit gray scale, and taken as proportional to solute concentration. Data were corrected for background intensity by averaging the radial profile over the 0.5-s prior to appearance of the bolus and subtracting the background from the bolus recording. The presence of red cells attenuates the bolus intensity along the microvessel centerline due to absorption of the excitation and emission, and light scattering. Peak intensity (with time) falls near the vessel wall due to dispersion of the bolus, and is delayed relative to the peak at the centerline.

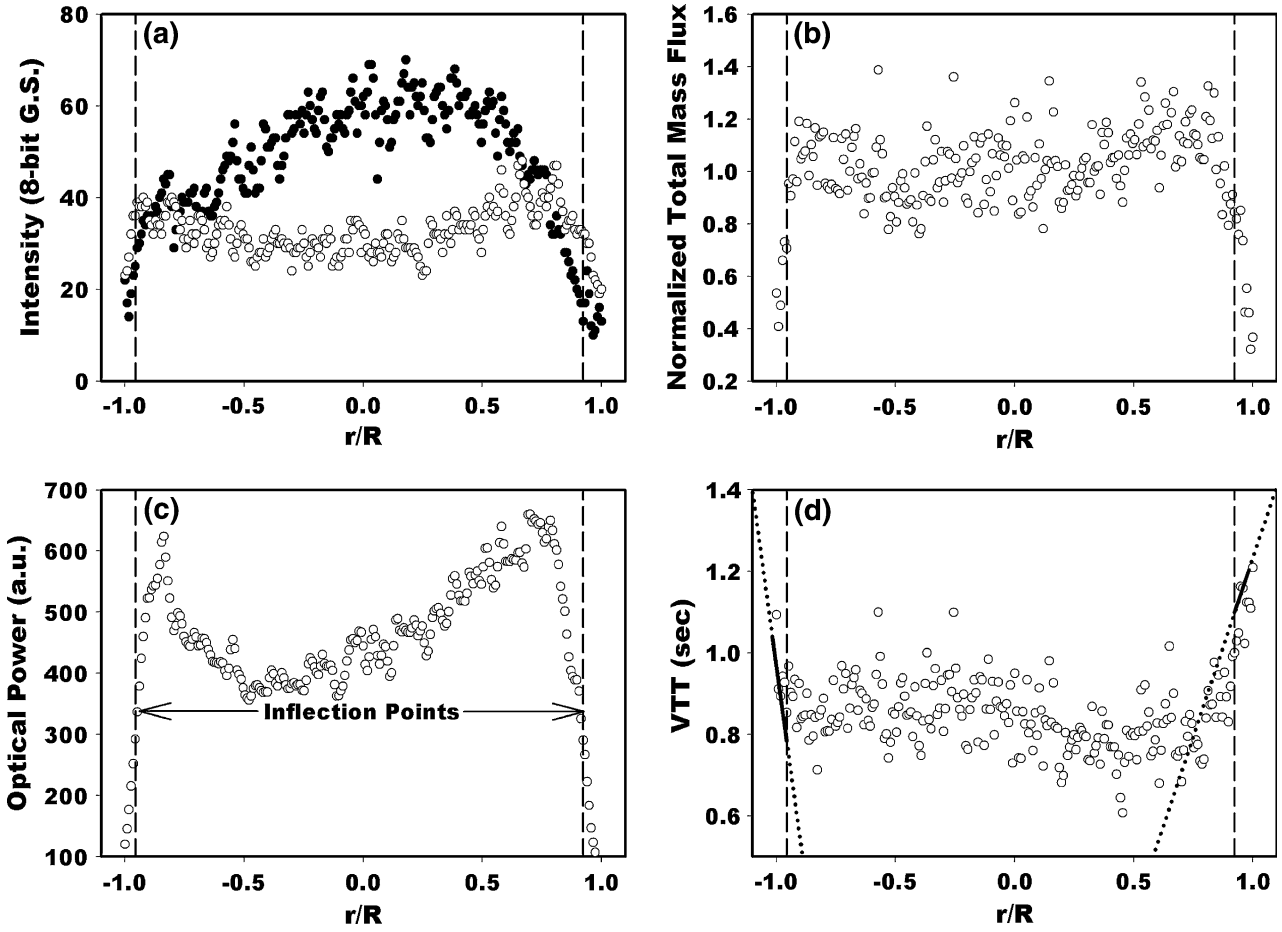

FIGURE 4. Representative experimental results extracted from the data of Fig. 3. (a) Radial distributions of fluorescent intensity when the centerline reaches its maximum (●) and when the near wall value attains its maximum (○). (b) Radial distribution of total mass flux ($\int I(t)dt$) normalized with respect to its centerline value. (c) Distribution of optical power calculated from the AC component of the intensity–time curve. The inflection point of optical power near the wall (dashed line shown in each panel) was taken as the boundary of a region containing the glycocalyx. (d) Radial profile of the calculated virtual transit time (VTT(r)). VTT has a uniformly low centerline value and rises rapidly from the inflection point to the wall ($r/R = 1$). The slope of VTT was determined by linear regression between the inflection point and vessel wall (shown in panel d as a solid line between the inflection point and wall, and dotted line beyond).

indicator with its dispersion along the axis of the vessel. The total mass passing the near-wall region between the EC and IP is 50% or less of the centerline, despite the fact that the indicator molecule is well mixed with plasma when entering the post-capillary venule. This behavior is consistent with diffusion of the indicator from the glycocalyx toward the center region when its concentration is higher than outside of the glycocalyx layer, at the trailing edge of the bolus, as illustrated in panel (a).

The optical power calculated from the a/c component of each intensity time curve along the vessel radius is shown in Fig. 4c. The inflection point (IP) was obtained by fitting a cubic spline to the descending edges of the radial optical power curve, and then finding the location of the zero second derivative. Under control conditions with FITC, the distance between the IP and plasma membrane of the endothelium (EC) averaged 0.90 μm, as summarized in Table 1. In contrast, the distance from the edge of the core of RBCs to the EC averaged 1.77 μm, as obtained from brightfield images of each venule. In all cases studied, the IP was typically on the order of 1 μm from the EC and half-way between the edge of the RBC core and EC.

The radial distribution of VTT(r) is shown in Fig. 4d for this representative venule. Within the central region of the vessel (for $r/R < 0.8$) VTT remained fairly flat across the entire core region, possibly as a result of the blunted velocity profile.[22] The VTT value increased dramatically when approaching the wall, primarily due to the reduction of velocity near the wall and attains a maximum value at the wall. Because of the noise level in the value of VTT(R), it was difficult

TABLE 2. Summary of basic *in vivo* measurements.

	Number of vessels	Number of bolus injections	Venule diameter (μm)	Velocity (mm/s)	VTT(R) (s)
(a) FITC					
Control	9	51	24.88 ± 4.09	2.83 ± 1.03	1.49 ± 0.26
fMLP	9	51		2.26 ± 1.19	1.59 ± 0.38*
(b) Dextran-70					
Control	5	27	25.72 ± 3.8	2.37 ± 0.61	1.35 ± 0.34
fMLP	5	27		2.01 ± 0.92	1.42 ± 0.27†

Values shown are mean ± SD for venular diameter, centerline RBC velocity and virtual transit time (Eq. 1) evaluated by extrapolating VTT(r) to the wall, $r = R$. VTT(R) not significantly different from control, t-test: *$p = 0.124$, †$p = 0.406$.

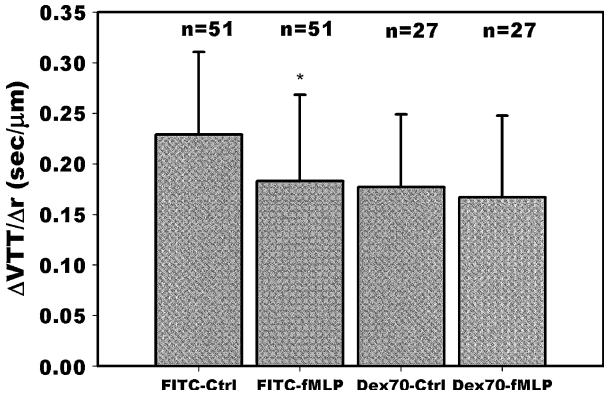

FIGURE 5. Comparison of slopes of the measured VTT(r), ΔVTT/Δr, for dispersion of FITC and FITC-Dextran 70 during superfusion of the mesentery under control conditions (Ringer's solution) and with 10^{-7} M fMLP-Ringer's solution (fMLP). For FITC, ΔVTT/Δr decreased significantly from 0.23 ± 0.08 SD to 0.18 ± 0.09 SD s/μm following fMLP superfusion, *$p < 0.05$. For boli of FITC-Dextran-70 ΔVTT/Δr did not change significantly, from control to fMLP and averaged 0.18 ± 0.07 SD and 0.17 ± 0.08 SD s/μm, respectively. The number of measurements (n) is shown for multiple boli in 9 venules.

to consistently identify a near wall value of VTT for analysis of dye transport through the glycocalyx. As shown in Table 2, values of VTT extrapolated to the wall ($r = R$), did not show a significant change between control and fMLP treatments. In contrast, however, the slope of VTT(r) between the inflection point (IP) of the optical power and the wall (ΔVTT/Δr) gave a consistent measure of the behavior of VTT near the wall, obtained by linear regression of the computed VTT(r) vs. r, as shown by the dashed lines in Fig. 4d. For all 156 measurements made, linear regressions of VTT near the wall had an average correlation coefficient (r) of 0.89 ± 0.07 SD and each regression slope was statistically significant (t-test, $p < 0.05$).

Measurements of the slope of the virtual transit time (ΔVTT/Δr) for two different size solutes, FITC and FITC-Dx70, are shown in Fig. 5 for 9 and 5 venules, respectively, prior to and following superfusion of the tissue with fMLP. The number of bolus infusions is given in Fig. 5, and statistics on venule diameters and mean RBC velocity are presented in Table 2. For FITC, ΔVTT/Δr fell significantly from 0.23 ± 0.08 SD to 0.18 ± 0.09 SD s/μm following fMLP (t-test, $p < 0.05$) presumably due to shedding of components of the glycocalyx. In contrast, ΔVTT/Δr for the Dx70 was significantly less than that for FITC and was not affected by shedding of the glycocalyx, thus suggesting that the larger Dx70 did not penetrate the glycocalyx significantly as the bolus traversed the venule. Statistical analysis of these data on a per vessel basis (i.e. 9 and 5 venules for FITC and Dx70, respectively) using average values of ΔVTT/Δr for each venule, revealed similar results. Due to variations in the 3-D shape of the vessel, its planar orientation (vessels were not always strictly horizontal), heterogeneity of the glycocalyx along the length of a venule, and the limitations in optical resolution, it was virtually impossible to perform repeated measurements at the same location. Hence, the statistical analysis was performed on the basis of the total number of measurements and each measurement was weighted individually.

Numerical Simulations

Results of a representative simulation of transmission of a bolus of small solutes through a tube are presented in Fig. 6. The simulation was performed using *in vivo* intensity–time curves averaged over five radial pixels on the centerline of a venule and applied uniformly across the entrance of the tube (shown in inset of Fig. 6), with specified values of δ, D_{eff} and K_{r}. For this simulation, the thickness of the glycocalyx was assumed to be 5% of the vessel radius, which for a 30 μm vessel would correspond to $\delta = 0.8$ μm. As in the case of the experimental measurements, a progressive delay of the intensity time curve is indicated by a delayed peak and prolonged tail in the indicator concentration *vs* time curve at the wall ($r/R = 1$).

Illustrated in Fig. 7 are the radial distributions of the computed solute concentration (panel a), normalized total (cumulative) mass flux (panel b), optical power (panel c) and virtual transit time (VTT) (panel d).

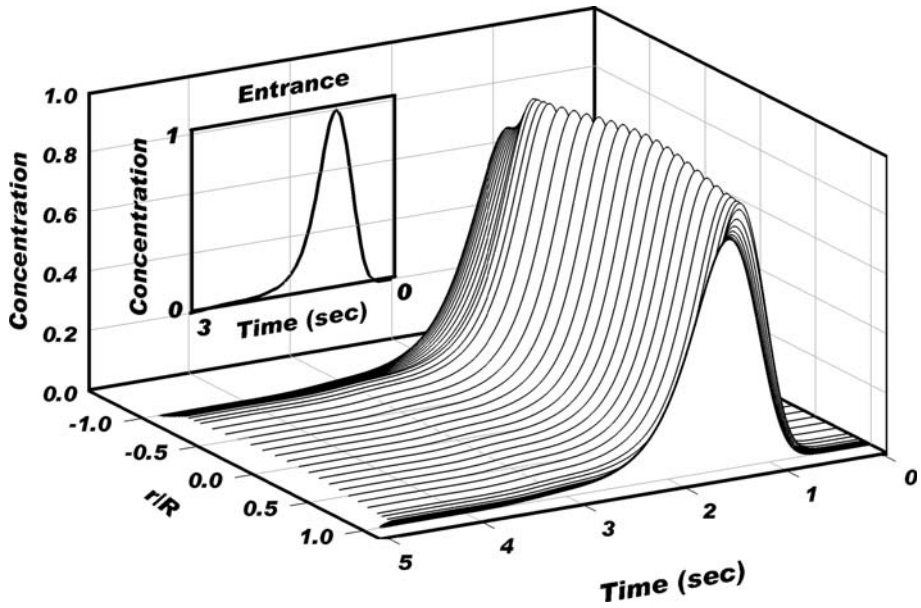

FIGURE 6. Computer simulation of dispersion of a bolus of solutes at 30 vessel diameters downstream of the entrance of a 30 μm diameter venule resulting from a specified concentration–time curve at the entrance (inset) taken from *in vivo* measurements. Shown are solute concentration–time (normalized by centerline values) curves over radius. The red cell core was assumed to be 1.7 μm from the vessel wall, the glycocalyx was 0.8 μm thick, the effective diffusion coefficient $D_{eff} = 0.2 \times 10^{-8}$ cm^2/s and the hydraulic resistivity $K_r = 10^{10}$ dyn·s/cm^4. The simulation replicates the gross features of the *in vivo* measurements, as evidenced by the attenuated and delayed peak concentration within the glycocalyx.

All four distributions reveal trends similar to those acquired *in vivo* (Fig. 4), with slight differences due to the absence of discrete RBC's in the simulation. The simulated total mass flux (Fig. 7b) appears much more parabolic compared with the *in vivo* measurements (Fig. 4b) because the light scattering by RBCs attenuates the fluorescence excitation and emission and thus disrupts the proportionality between light intensity and dye concentration. In contrast, measurements of fluorescence emission are affected less within the plasma layer and glycocalyx. It should be noted that light scattering effects become accentuated with high numerical aperture objectives (needed for higher spatial resolution) and play a lesser role with lower magnification-numerical aperture objectives.[12] The vertical dashed lines in each panel represent the radial location of the inflection point in the optical power distribution (panel c). In all simulations, the inflection point occurred between the EC and edge of the RBC core (r_c), and was typically within $\pm 6\%$ of r_c, for assumed thicknesses ranging from 100 nm to 1 μm. The radial distribution of VTT(r) falls rapidly within the layer bounded by the RBC core with its maximum slope at the inflection point. Near the wall ($r/R = 1$), VTT(r) approaches a constant value as dVTT(r)/dr approaches 0. As suggested by Eq. (1), the slope of $c(r)$ and dVTT/dr approach zero near the wall to reflect zero radial mass transfer ($\partial c/\partial r = 0$). Thus, in light of the bounded nature of the slope of VTT(r) within the plasma layer, its absolute value was used as an indicator of the behavior of VTT(r) and transit of solutes through the glycocalyx.

Parametric numerical simulations corresponding to the three independent variables, δ, K_r and D_{eff} were performed to describe the variation of ΔVTT/Δr over a range that includes its measured values, as shown in Fig. 8. Each panel corresponds to the indicated thickness of the glycocalyx (δ) and shows a set of parametric curves for a range of values in D_{eff} normalized with respect to the free diffusion coefficient of FITC. In each case, the variation of ΔVTT/Δr was relatively insensitive to large variations in K_r for $10^5 < K_r < 10^{14}$ dyn·s/cm^4 (shown only up to 10^{10} for clarity). Most strikingly, in order to approach a range of ΔVTT/Δr similar to *in vivo* measurements, values of D_{eff} on the order of 0.003% of D_{free} were required for a 100 nm thick glycocalyx and 0.5% of D_{free} for a 700 nm thick glycocalyx. Thus, the thinner the glycocalyx, the greater the reduction in the effective diffusion coefficient must be in order to slow down the movement of solutes through the layer to yield the indicated slope of VTT near the wall.

Simulations corresponding to control and fMLP values of ΔVTT/Δr are presented in Fig. 9 for four specific thicknesses of the glycocalyx ranging from 100 to 700 nm. These computations illustrate the possible range of concurrent changes in D_{eff} and K_r that would result in the measured change in ΔVTT/Δr for a given thickness. For example, given a nominal thickness of

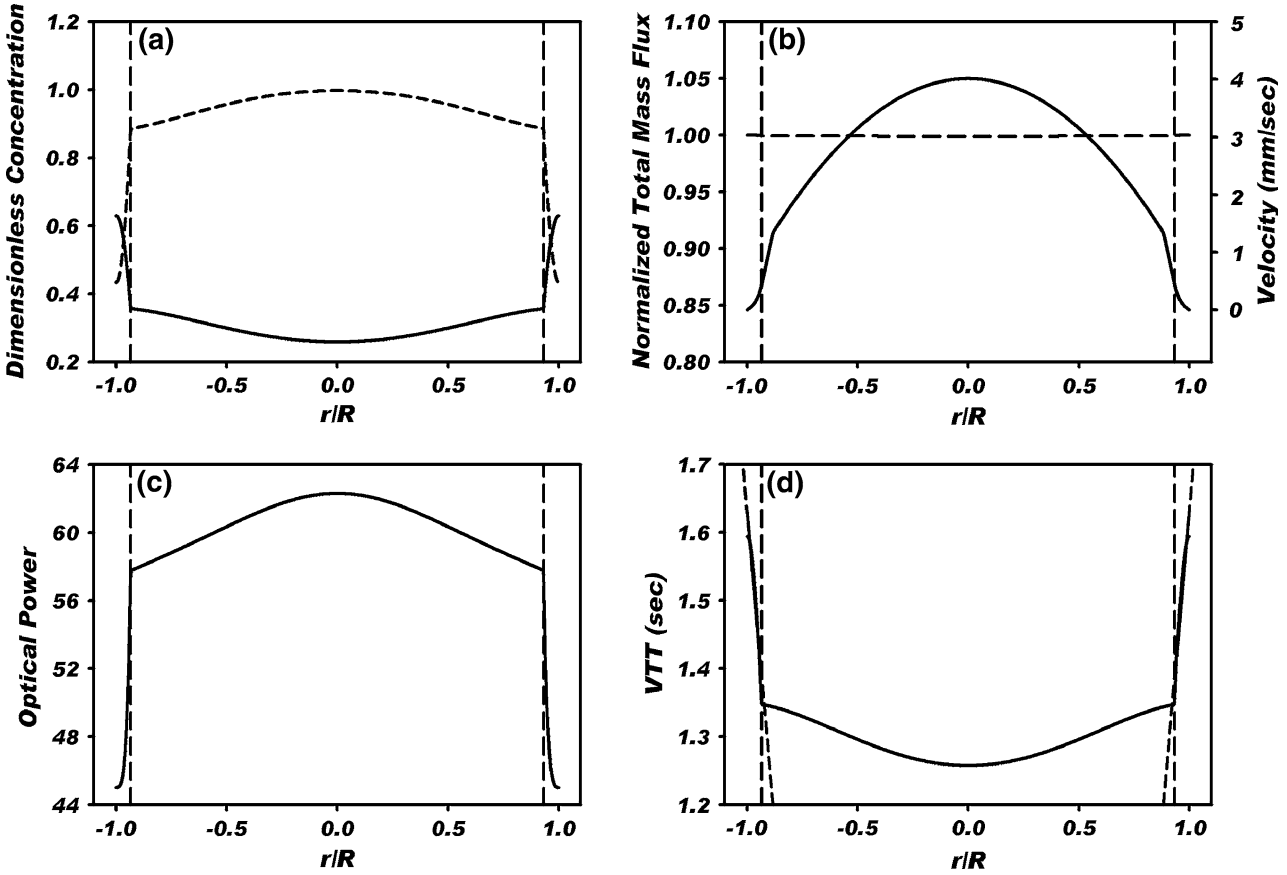

FIGURE 7. Radial distribution of parameters for the simulated bolus transport shown in Fig. 6. Two vertical dashed lines in each panel indicate the location of the inflection point in the optical power. (a) Radial distribution of dimensionless concentration of the indicator molecule. The dash line corresponds to the time when centerline concentration attains its maximum value, and the solid line refers to the time when the near-wall layer reaches its maximum. (b) Centerline-normalized total mass flux (dashed line) and velocity profile (solid line). The velocity begins to fall off sharply at the boundary of the red cell core with increasing *r*/*R*, and reveals an inflection point within the glycocalyx at $\approx\delta/2$. (c) Radial distribution of the optical power. (d) VTT(*r*), where linear regression lines in the region 1-μm from the wall (solid line, extended with dash lines) were used to obtain the slope ΔVTT(*r*)/Δr. These results are consistent with the *in vivo* measurements, although the location of the inflection point for the optical power occurs within ±6% of the location of edge of the red cell core.

500 nm (Fig. 9c) the response to fMLP would be typified by moving from one point on the lower (solid) curve to a point on the upper (dashed) curve. Assuming that structural elements of the glycocalyx are lost due to enzymatic shedding, it would appear logical to envisage a reduction in K_r from, for example, its maximum value of 10^{10} dyn·s/cm^2 to as low 10^5 dyn·s/cm^2 with an attendant increase in D_{eff} from 2.5×10^3 to about 2.9×10^3 times the free diffusion coefficient, i.e. a 15% increase in D_{eff}. If K_r remains constant at 10^{10} dyn·s/cm^2 in response to fMLP, then the solution could be obtained with roughly a 10% greater increase in D_{eff} from 2.5 to $3.2 \times 10^3 \times D_{free}$. Thus, one may conclude that very small changes in the ability of the solute to diffuse through the glycocalyx have the greatest impact on its transport.

Simulations also indicated that large variations of the bulk velocity of blood flow (from 2 to 10 mm/s) has only a small effect (±5%, results not shown) on ΔVTT/Δr, indicating that the near-wall velocity rather than core velocity affects transport through the glycocalyx layer.

DISCUSSION

The present study has employed a variant of the indicator dilution technique to probe for changes in the endothelial glycocalyx during a model inflammatory response in post-capillary venules. The dispersion of solutes flowing through a uniform tube of circular cross-section is a classic problem that has been extensively studied since the seminal studies of Sir Geoffrey Taylor.[32] As shown therein, the axial dispersion of a bolus of solute in steady flow is dependent upon convective transport parallel to the axis of the tube and

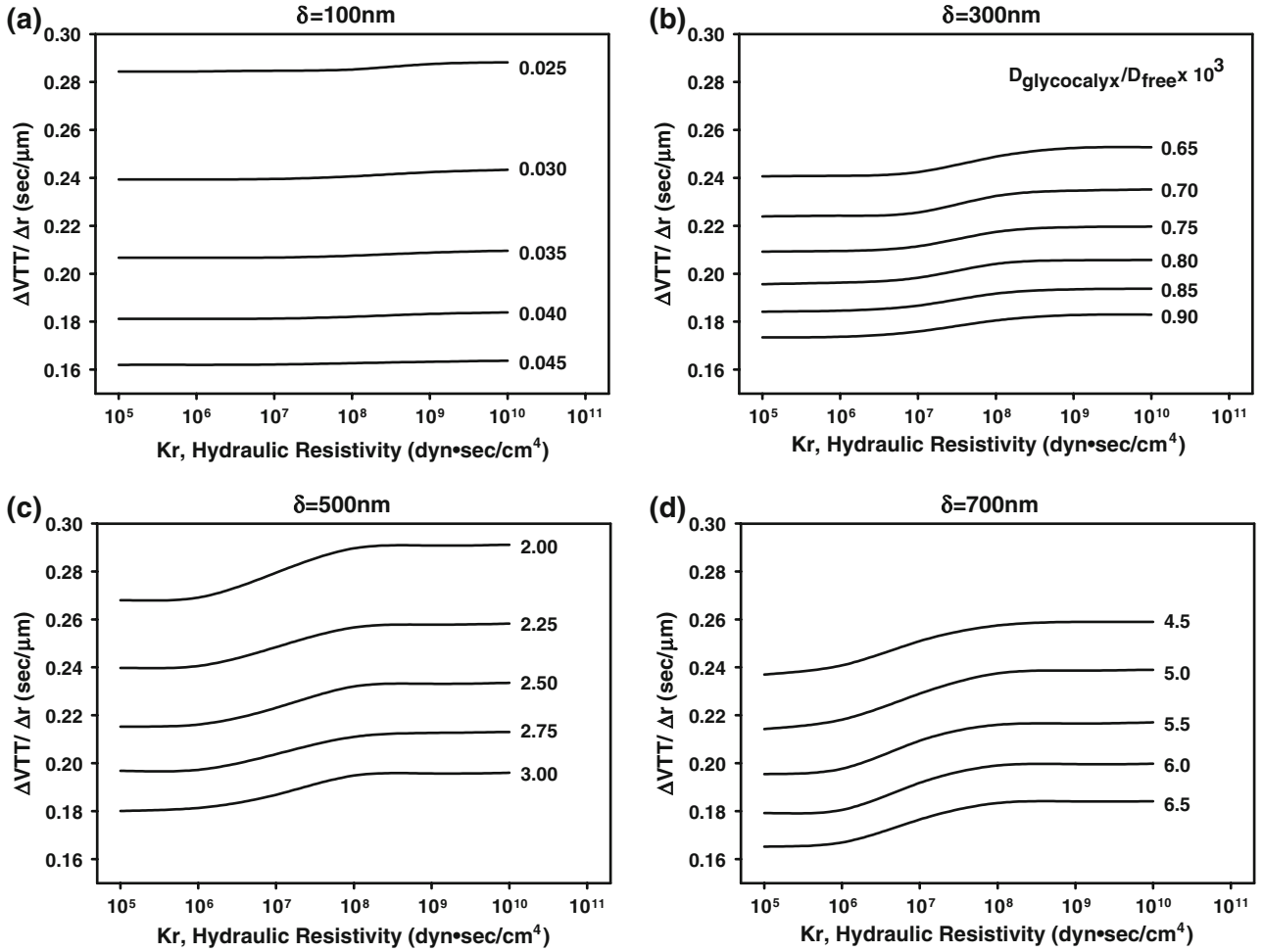

FIGURE 8. Parametric plots derived from the computer simulations illustrating the slope $\Delta VTT/\Delta r$ as a function of hydraulic resistivity of the glycocalyx (K_r) for specified values of the effective diffusion coefficient ($D_{glycocalyx}/D_{free}$) of a small solute in the surface layer, for four thicknesses of the glycocalyx. The slope of VTT is relatively constant over the indicated range of K_r and is much more sensitive to diffusion coefficient within the glycocalyx of a given thickness.

molecular diffusion in the radial direction. The relative contributions of convection and diffusion in affecting indicator dispersion have been characterized mathematically by Taylor.[32,33] Given a vessel of length L and radius a, and a steady flow with mean velocity U, radial diffusion of a solute with diffusion coefficient D will dominate convection when $L/U \gg 2a^2/3.8^2D$ (Taylor's condition B). Given values typical of postcapillary venules ($L = 0.5$ mm, $U = 1$ mm/s, $a = 0.015$ mm, $D_{FITC} = 2.7 \times 10^{-4}$ mm^2/s) values for these terms are 0.5 and 0.12 s, respectively. Thus, for an idealized uniform fluid devoid of blood cells the dispersion of a bolus of FITC would depend upon both diffusion and the mean velocity of flow. However, in the case of *in vivo* microvessels, it is well recognized that the presence of RBCs in the central core enhances mixing of plasma borne solutes and results in an effective diffusion coefficient that is much greater than in a quiescent solvent.[30] Studies of the transit time of fluorescent macromolecules and red cells through successive branches of the microvasculature have revealed that mixing within the central core of RBCs occurs rapidly and that the Stewart–Hamilton relationship can be used to give a realistic measure of mean transit time of fluorescently tagged RBCs and plasma that is consistent with the average Fahraeus effect within a microvascular network.[9]

The use of first moment of indicator concentration as a probe for the speed with which solutes negotiate the glycocalyx departs from the traditional Stewart–Hamilton approach. A discrete reference for the injection time and assurance of conservation of the mass of indicator were not used. Instead, the VTT was based upon the total concentration of indicator passing through the observation site with both integrals in Eq. (1) ranging from the time of first appearance of the indicator in the RBC core to its full duration. In the context of the Stewart–Hamilton approach, the first

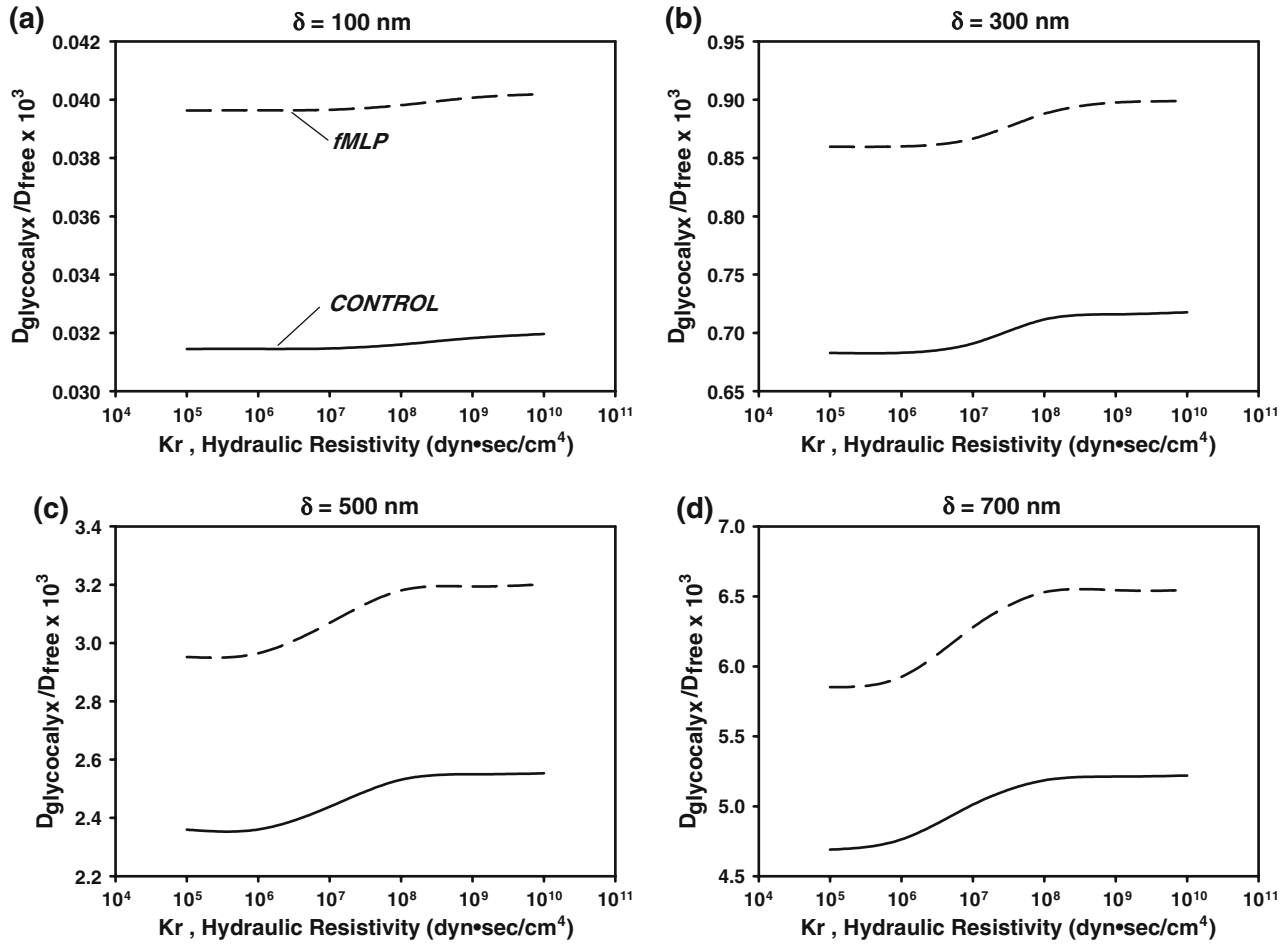

FIGURE 9. Simulations representing curves of constant $\Delta VTT/\Delta r$ for control (solid line) and fMLP (dashed line) treatments (FITC, Fig. 5) for four assumed thicknesses of the glycocalyx: 100, 300, 500 and 700 nm. Radial diffusion of the solute through the glycocalyx has the greatest effect on the slope of the virtual transit time at the wall and dominates changes in response to superfusion with fMLP.

moment corresponds to the mean value of the indicator which exhibits a temporal distribution that represents the frequency distribution of transit times through all pathways taken by the indicator from injection to observation sites.[13] In the current approach VTT corresponds to the time weighted average of the observed indicator, normalized with respect to the total indicator passing through the observation site. Attempts to use higher moments, such as the second moment, indicative of the variance of the indicator, were confounded by noise inherent to the low amplitude signals near the microvessel wall and therefore were not productive. The numerical simulations (Figs. 6–9) provide evidence that the slope (dVTT/dr) at the wall was sensitive to the diffusion coefficient (D_{eff}) and hydraulic resistance (K_r) in the glycocalyx.

Simulations of indicator dispersion under conditions similar to those observed *in vivo* revealed that the effective diffusion coefficient within the core does not significantly affect dispersion of the indicator within the plasma layer. Namely, variation of the slope of the virtual transit time VTT(r), at the wall, reveals that it is insensitive to the magnitude of D_{eff} within the RBC core and depends mainly on D_{eff} within the plasma layer and glycocalyx. Hence, to gain insight into the behavior of $\Delta VTT/\Delta r$ with D_{eff}, K_r and δ, the numerical simulations were performed for mean bulk velocities and vessel geometries similar to those observed *in situ*.

Changes in the Thickness, Permeability and Diffusion Coefficient

Using numerical simulations to interpret the *in vivo* response to the fMLP model of inflammation, suggests that changes in K_r have a lesser effect compared to D_{eff} or δ, as indicated by the simulations shown in Figs. 6–9.

The relative insensitivity of $\Delta VTT/\Delta r$ to K_r suggests that the *in vivo* measurements may be much more sensitive to the diffusion of solutes through the layer in the radial direction. Although structural and composition changes in the glycocalyx may affect K_r, it appears that restrictive flow of the solvent is not sufficient to impede the diffusional transport of small solutes through the glycocalyx. These results are summarized in Fig. 10 where parametric curves are shown for the calculated decrease in δ (nm) required for the measured changes in $\Delta VTT/\Delta r$ from control to fMLP treatments. As indicated, for low values of D_{eff}, a small 10–20 nm decrease in δ is needed over a broad range of K_r. That is, the more compact the glycocalyx, with greater restriction of the diffusion of solutes as pathways become narrower compared to the size of the solute, then the more sensitive the solution becomes to small reductions in the total thickness. In contrast, for a relatively less compact glycocalyx, with greater diffusivity of solutes, a greater reduction in thickness of the layer is required to affect the change in $\Delta VTT/\Delta r$.

Implications for a Structural Model of the Glycocalyx

To date, *in vivo* studies of the transvascular exchange of fluid have been unable to separate the dynamics of hydraulic permeability between the glycocalyx and its accompanying endothelial and tissue barrier, except by physically modifying the endothelial surface layer to observe changes in the radial permeability to fluid, L_p.[2] The current approach affords the opportunity to characterize permeability of the glycocalyx in the radial direction without the influence of the endothelial barrier itself. In general, the hydraulic permeability of the glycocalyx in radial and axial directions may be related by drawing upon the definition of L_p which is defined as the solvent flux per unit area, Jv/A, divided by the pressure drop, i.e. $L_p = J_v/A\Delta P$.[14] Upon consideration of conservation of momentum from Eq. (3) for an average flow parallel to the vessel wall within the glycocalyx with $\partial u/\partial r = 0$ then for equivalent pressure gradients in radial and axial directions, $L_p K_r \delta = 1$. Assuming that the hydraulic resistivity in axial and radial directions are equal, i.e. that the glycocalyx is isotropic, the values of K_r spanned in the present simulations (Figs. 8–10) bracket experimental measurements suggested by *in vivo* measurements of L_p. For example, for $K_r = 10^5$ dyn·s/cm^4 and $\delta = 100$ nm, and $K_r = 10^{14}$ dyn·s/cm^4 and $\delta = 700$ nm, then L_p would range from 10^3 to 10^{-7} cm/s/cmH_2O, respectively.

Direct measurement of L_p using the Landis technique in frog capillaries have resulted in a value of 2×10^{-7} cm/s/cmH_2O measured in frog mesentery by Adamson.[2] In these experiments, capillaries were perfused with pronase to strip off the glycocalyx resulting in a measurement of L_p equal to 4.9×10^{-7} cm/s/cmH_2O. Assuming that the hydraulic resistance is the result of two serial resistive elements (i.e. with resistance $= 1/L_p$) one may calculate L_p for the glycocalyx equal to 3.38×10^{-7} cm/s/cmH_2O. Thus, for a thickness $\delta = 500$ nm, *in vivo* measurements[2] suggest that $K_r = 5.8 \times 10^{13}$ dyn·s/cm^4. The present simulations suggest that the effect of hydraulic resistance on solute transport reaches an asymptote for $K_r > 10^8$ dyn·s/cm^4 in order to attain the measured slope of VTT(r) at the wall (Fig. 10). That is, axial water movement through the glycocalyx has little effect on the diffusion limited transport of small solutes in the radial direction. For $K_r < 10^8$ dyn·s/cm^4, with increasing thickness of the layer, the greater the hydraulic resistance in the layer, the larger D_{eff} must be in order to attain a solution that matches experimental measurements of the slope of VTT(r) (Fig. 10). Hence, reductions in the near wall axial fluid flow with increased K_r tend to limit the axial dispersion of small solutes, which parallels Taylor's analysis of dispersion from convection alone.[32]

The effective diffusion coefficient, D_{eff}, appears to rise for all values of δ to reflect the changes in VTT attendant to the topical application of fMLP. As shown previously, enzymatic shedding of glycans occurs due to the activation of G-protein coupled receptors on the endothelium.[16] These structural changes in the density of proteoglycans and GAGs may serve to increase the effective pore size through which small solutes can diffuse. The effect of fMLP on the relationship between D_{eff} and K_r for a given δ (Fig. 10) is consistent with direct measurements of L_p

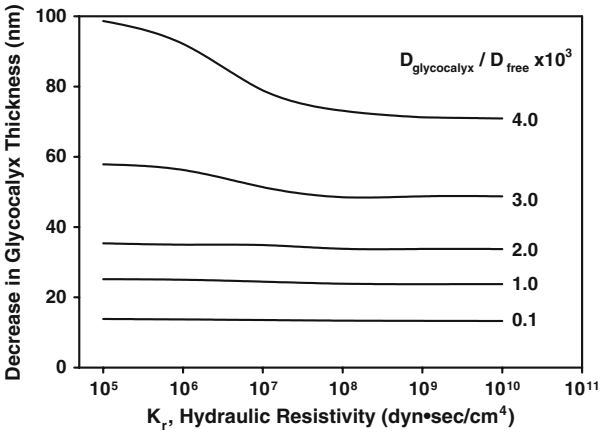

FIGURE 10. Calculated decrease in thickness of the glycocalyx (δ) required to produce the increase in $\Delta VTT/\Delta r$ from control to fMLP treatments for a given value of K_r and diffusion coefficient in the glycocalyx. D_{free} is the free diffusion coefficient of FITC in aqueous media. At higher levels of K_r the required decrease in δ approaches an asymptote that is dependent on diffusion coefficient in the glycocalyx.

in microvessel where it has been shown that L_p is not affected by perfusion of microvessels with fMLP.[39] Hence the apparent uniform rise in D_{eff} over several orders of magnitude of K_r most likely reflects the dominance of D_{eff} in dispersion of the solutes.

The present measurements of a bolus of FITC traveling axially through a microvessel occur within a short period of time on the order of 1–4 s. In contrast, following systemic infusion of a large bolus of FITC and tracking the progress of the dye front in the plasma layer as it approached the endothelium,[36] the time course of FITC infiltrating the glycocalyx has been shown to occur with a half-time of 11 min. Based upon their measurements, a diffusion coefficient may be roughly estimated by assuming that the dye front moves at the speed of the average concentration of a linear radial gradient of solute within the glycocalyx to yield a value of $D_{eff} \approx 2 \times 10^{-10}$ cm^2/s. This magnitude compares favorably with the simulation value corresponding to the measured $\Delta VTT/\Delta r$ and assuming $\delta = 500$ nm for which $D_{eff} \approx 65 \times 10^{-10}$ cm^2/s (Fig. 9c with $K_r = 10^{14}$). For comparison, direct measurements of D_{eff} for sodium fluorescein in connective tissue[17] yielded a value of 20×10^{-7} cm^2/s. Thus, the glycocalyx appears to have a relatively more compact molecular structure that limits the transvascular transport of small solutes. The increases in D_{eff} attendant to superfusion of the tissue with fMLP (Fig. 10), is thus consistent with a loss of glycans and increased pore size for the movement of solutes. The inability of macromolecules to penetrate the glycocalyx, as evidenced here by the inability of Dx70 to exhibit a change in $\Delta VTT/\Delta r$ in response to fMLP, is consistent with the previously shown inability of Dx70 to infiltrate the glycocalyx.[36]

The small values of D_{eff} found here under control conditions ($D_{eff}/D_{free} = 2.5 \times 10^{-3}$) may be the result of the small porosity of the glycocalyx and accompanying solute interactions with its structure. The effective diffusion coefficient of small solutes in the glycocalyx has been studied extensively in light of the hydrodynamic diameter of solutes and the effective size of discrete pores or a fiber-matrix of specified void volume.[5,14] Assuming discrete cylindrical pores, then for FITC with a Stokes–Einstein radius of 0.8 nm and using the relations given in Nugent and Jain,[18] a pore size <2 nm would be necessary to match D_{eff} obtained from $\Delta VTT/\Delta r$. Analysis of ultrastructural data observed by electron microscopy suggest a hypothetical pore size of 10 nm is prevalent in the glycocalyx consisting of 10 nm diameter fibers spaced at 20 nm intervals.[31] Based upon these dimensions, application of the pore theory[18] to control conditions would give a diffusion coefficient for FITC of $0.7D_{free}$. Application of the fiber-matrix theory[18] suggests a value of $D_{eff} \approx 0.3D_{free}$. These disparities with the estimates of D_{eff} herein suggest that the present indicator dispersion method may reflect the tortuosity and heterogeneity of solute pathways, charge effects and levels of hydration of the *in situ* glycocalyx, all of which could yield much smaller values than estimates based upon morphological structure.

In summary, the present study has undertaken to develop a new method for exploring the structure of the endothelial glycocalyx using techniques of indicator dispersion. Measurements of the dispersion of FITC were interpreted in terms of the gradient of a virtual transit time at the microvessel wall and used to explore the relationship between diffusion of solutes and hydraulic resistance within the glycocalyx using an idealized computational model. It has been demonstrated that the effective diffusion coefficient is the dominant determinant of solute dispersion and reveals values consistent with *in vivo* observations of infiltration of fluorescently labeled solutes into the glycocalyx.

ACKNOWLEDGMENTS

This work was supported by NIH R01 HL-39286. The authors thank Ms. Anne Lescanic for her technical assistance.

REFERENCES

[1]Abrahamsson, T., U. Brandt, S. L. Marklund, and P. O. Sjoqvist. Vascular bound recombinant extracellular superoxide dismutase type C protects against the detrimental effects of superoxide radicals on endothelium-dependent arterial relaxation. *Circ. Res.* 70:264–271, 1992.

[2]Adamson, R. H. Permeability of frog mesenteric capillaries after partial pronase digestion of the endothelial glycocalyx. *J. Physiol.* 428:1–13, 1990.

[3]Adamson, R. H., and G. Clough. Plasma proteins modify the endothelial cell glycocalyx of frog mesenteric microvessels. *J. Physiol.* 445:473–486, 1992.

[4]Constantinescu, A. A., H. Vink, and J. A. Spaan. Endothelial cell glycocalyx modulates immobilization of leukocytes at the endothelial surface. *Arterioscler. Thromb. Vasc. Biol.* 23:1541–1547, 2003.

[5]Curry, F. E., and C. C. Michel. A fiber matrix model of capillary permeability. *Microvasc. Res.* 20:96–99, 1980.

[6]Desjardins, C., and B. R. Duling. Heparinase treatment suggests a role for the endothelial cell glycocalyx in regulation of capillary hematocrit. *Am. J. Physiol.* 258:H647–H654, 1990.

[7]Gouverneur, M., B. Berg, M. Nieuwdorp, E. Stroes, and H. Vink. Vasculoprotective properties of the endothelial glycocalyx: effects of fluid shear stress. *J. Intern. Med.* 259:393–400, 2006.

[8]Huxley, V. H., and D. A. Williams. Role of a glycocalyx on coronary arteriole permeability to proteins: evidence from

enzyme treatments. *Am. J. Physiol. Heart Circ. Physiol.* 278:H1177–H1185, 2000.
[9]Lipowsky, H. H., L. E. Cram, W. Justice, and M. J. Eppihimer. Effect of erythrocyte deformability on in vivo red cell transit time and hematocrit and their correlation with in vitro filterability. *Microvasc. Res.* 46:43–64, 1993.
[10]Lipowsky, H. H., and B. W. Zweifach. Application of the "two-slit" photometric technique to the measurement of microvascular volumetric flow rates. *Microvasc. Res.* 15: 93–101, 1978.
[11]Luft, J. H. Fine structures of capillary and endocapillary layer as revealed by ruthenium red. *Fed. Proc.* 25:1773–1783, 1966.
[12]McKay, C. B., and H. H. Lipowsky. Arteriovenous distribution of transit times in cremaster muscle of the rat. *Microvasc. Res.* 36:75–91, 1988.
[13]Meier, P., and K. Zierler. On the theory of the indicator-dilution method for measurement of blood flow and volume. *J. Appl. Physiol.* 6:731–744, 1954.
[14]Michel, C. C., and F. E. Curry. Microvascular permeability. *Physiol. Rev.* 79:703–761, 1999.
[15]Mulivor, A. W., and H. H. Lipowsky. Role of glycocalyx in leukocyte-endothelial cell adhesion. *Am. J. Physiol. Heart Circ. Physiol.* 283:H1282–H1291, 2002.
[16]Mulivor, A. W., and H. H. Lipowsky. Inflammation- and ischemia-induced shedding of venular glycocalyx. *Am. J. Physiol. Heart Circ. Physiol.* 286:H1672–H1680, 2004.
[17]Nugent, L. J., and R. K. Jain. Plasma pharmacokinetics and interstitial diffusion of macromolecules in a capillary bed. *Am. J. Physiol.* 246:H129–H137, 1984.
[18]Nugent, L. J., and R. K. Jain. Pore and fiber-matrix models for diffusive transport in normal and neoplastic tissues. *Microvasc. Res.* 28:270–274, 1984.
[19]Oohira, A., T. N. Wight, and P. Bornstein. Sulfated proteoglycans synthesized by vascular endothelial cells in culture. *J. Biol. Chem.* 258:2014–2021, 1983.
[20]Pearson, M. J., and H. H. Lipowsky. Influence of erythrocyte aggregation on leukocyte margination in postcapillary venules of rat mesentery. *Am. J. Physiol. Heart Circ. Physiol.* 279:H1460–H1471, 2000.
[21]Periasamy, N., and A. S. Verkman. Analysis of fluorophore diffusion by continuous distributions of diffusion coefficients: application to photobleaching measurements of multicomponent and anomalous diffusion. *Biophys. J.* 75:557–567, 1998.
[22]Pittman, R. N., and M. L. Ellsworth. Estimation of red cell flow microvessels: consequences of the Baker-Wayland spatial averaging model. *Microvasc. Res.* 32:371–388, 1986.
[23]Potter, D. R., and E. R. Damiano. The hydrodynamically relevant endothelial cell glycocalyx observed in vivo is absent in vitro. *Circ. Res.* 102:770–776, 2008.
[24]Pries, A. R., T. W. Secomb, and P. Gaehtgens. The endothelial surface layer. *Pflugers Arch.* 440:653–666, 2000.
[25]Quinsey, N. S., A. L. Greedy, S. P. Bottomley, J. C. Whisstock, and R. N. Pike. Antithrombin: in control of coagulation. *Int. J. Biochem. Cell Biol.* 36:386–389, 2004.
[26]Reitsma, S., D. W. Slaaf, H. Vink, M. A. van Zandvoort, and M. G. Oude Egbrink. The endothelial glycocalyx: composition, functions, and visualization. *Pflugers Arch.* 454:345–359, 2007.
[27]Secomb, T. W., R. Hsu, and A. R. Pries. A model for red blood cell motion in glycocalyx-lined capillaries. *Am. J. Physiol.* 274:H1016–H1022, 1998.
[28]Sharan, M., and A. S. Popel. A two-phase model for flow of blood in narrow tubes with increased effective viscosity near the wall. *Biorheology* 38:415–428, 2001.
[29]Smith, M. L., D. S. Long, E. R. Damiano, and K. Ley. Near-wall micro-PIV reveals a hydrodynamically relevant endothelial surface layer in venules in vivo. *Biophys. J.* 85:637–645, 2003.
[30]Spaeth, E. E., and S. K. Friedlander. The diffusion of oxygen, carbon dioxide, and inert gas in flowing blood. *Biophys. J.* 7:827–851, 1967.
[31]Squire, J. M., M. Chew, G. Nneji, C. Neal, J. Barry, and C. Michel. Quasi-periodic substructure in the microvessel endothelial glycocalyx: a possible explanation for molecular filtering? *J. Struct. Biol.* 136:239–255, 2001.
[32]Taylor, G. Dispersion of soluble matter in solvent flowing slowly through a tube. *Proc. R. Soc. Lond. Ser. A* 219:186–203, 1953.
[33]Taylor, G. Conditions under which dispersion of a solute in a stream of solvent can be used to measure molecular diffusion. *Proc. R. Soc. Lond. Ser. A* 225:473–477, 1954.
[34]Vink, H., A. A. Constantinescu, and J. A. Spaan. Oxidized lipoproteins degrade the endothelial surface layer: implications for platelet-endothelial cell adhesion. *Circulation* 101:1500–1502, 2000.
[35]Vink, H., and B. R. Duling. Identification of distinct luminal domains for macromolecules, erythrocytes, and leukocytes within mammalian capillaries. *Circ. Res.* 79:581–589, 1996.
[36]Vink, H., and B. R. Duling. Capillary endothelial surface layer selectively reduces plasma solute distribution volume. *Am. J. Physiol. Heart Circ. Physiol.* 278:H285–H289, 2000.
[37]Weinbaum, S., X. Zhang, Y. Han, H. Vink, and S. C. Cowin. Mechanotransduction and flow across the endothelial glycocalyx. *Proc. Natl. Acad. Sci. USA* 100:7988–7995, 2003.
[38]Yayon, A., M. Klagsbrun, J. D. Esko, P. Leder, and D. M. Ornitz. Cell surface, heparin-like molecules are required for binding of basic fibroblast growth factor to its high affinity receptor. *Cell* 64:841–848, 1991.
[39]Zhu, L., V. Castranova, and P. He. fMLP-stimulated neutrophils increase endothelial [Ca2+]i and microvessel permeability in the absence of adhesion: role of reactive oxygen species. *Am. J. Physiol. Heart Circ. Physiol.* 288:H1331–H1338, 2005.
[40]Zuurbier, C. J., C. Demirci, A. Koeman, H. Vink, and C. Ince. Short-term hyperglycemia increases endothelial glycocalyx permeability and acutely decreases lineal density of capillaries with flowing red blood cells. *J. Appl. Physiol.* 99:1471–1476, 2005.